Tailoring Mechanical Properties and Ionic Conductivity of Poly(ionic liquid)-based Ion Gels by Tuning Anion Compositions

Takaichi Watanabe[a*], Yuna Mizutani[a], Carlos G. Lopez[b], and Tsutomu Ono[a*]

[a] Department of Applied Chemistry, Graduate School of Environmental, Life, Natural Science, and Technology, Okayama University, 3-1-1, Tsushima-naka, Kita-ku, Okayama, 700-8530, JAPAN

[b] Material Science and Engineering Department, The Pennsylvania State University, 80 Pollock Rd, 16801 State College, US

*Takaichi Watanabe (Email: wata-t@okayama-u.ac.jp, Phone & Fax: +81-86-251-8072)

*Tsutomu Ono (Email: tono@okayama-u.ac.jp, Phone & Fax: +81-86-251-8083)

KEYWORDS

Poly(ionic liquid), Anion exchange, Gel, Conductivity, Toughness

ABSTRACT

Poly(ionic liquid) (PIL)-based ion gels have emerged as promising materials for advanced electrochemical applications because of their excellent miscibility with ionic liquids (IL), tunable mechanical properties, and high ionic conductivity. Despite extensive studies on PIL-based ion gels, a comprehensive understanding of how different anion combinations in the system affect physicochemical properties is lacking. In this study, we systematically investigate the effect of different anion species, such as bis(trifluoromethanesulfonyl)imide (TFSI) and hexafluorophosphate (PF_6), on the mechanical, viscoelastic, and ion conductive behaviors of PIL-based ion gels. We investigate the interplay between

anion size, packing density, and polymer segmental dynamics by varying the anion composition in both the PIL network and IL component. Rheological analysis and uniaxial tensile testing results indicate that PF_6-containing ion gels exhibit enhanced higher Young's modulus because of their restricted chain mobility resulting in higher glass transition temperature (T_g). In addition, we confirm the anion exchange between PIL and IL during gel preparation and find that the mechanical and ion conductive properties of the gels are governed by the total molar ratio of anions in the gels. Our findings highlight that tuning the anion composition in PIL-based ion gels provides an effective strategy to tailor their performance, with potential applications for flexible electronics and solid-state electrochemical devices.

1. INTRODUCTION

Ion gels are soft materials composed of crosslinked polymer networks swollen with a large amount of ionic liquid (IL) (typically 40–60 wt% or higher). Incorporation of ILs imparts ion gels with a unique set of properties, including negligible vapor pressure, high thermal stability[1,2], flame resistance[3], high ionic conductivity[4], and selective CO_2 absorption capacity. The polymer matrix provides mechanical integrity and processability, enabling their integration into various functional devices. Consequently, ion gels have been successfully employed in strain sensors[5–7], actuators[8–10], supercapacitors[11–13], energy storage devices, and CO_2 separation membranes[14–17]. Combining hydrophobic polymer networks with hydrophobic ILs imparts superior stability to ion gels in humid and aqueous environemnts[18–21], broadening their applicability in separation membranes and soft electronic devices operating under extreme conditions (such as underwater or a wide temperature range). The physical properties of ion gels are controlled by the type of polymer, network structure, and IL content retained as a solvent. In ion gels that use acrylate-based polymers such as poly(methyl methacrylate), changing the ion species in the gel affects their physical properties including viscoelasticity, tensile strength, and self-healing performance even when the type of polymer and IL content remain the same[22,23]. Notably, altering the anion structure, rather than the cation significantly changes the mechanical strength[23].

Ion gels based on poly(ionic liquid) (PIL) networks have recently gained significant attention due to their

high thermal stability[24–27]. PILs feature covalently tethered ionic groups within their polymer backbone and exhibit excellent miscibility with ILs via the "like-dissolves-like" principle. This strong affinity leads to homogeneous gel structures with stable ionic pathways. The performance of PIL-based ion gels could be strongly influenced by the anion species present in both the PIL and IL components. Bis(trifluoromethanesulfonyl)imide (TFSI) and hexafluorophosphate (PF_6), two anions commonly used in PIL-based gels, differ significantly in their physicochemical characteristics. TFSI possesses a flexible structure and delocalized charge distribution, resulting in a lower glass transition temperature (T_g) and enhanced ion mobility. In contrast, PF_6, with its smaller ionic radius and stronger electrostatic interactions, promotes denser polymer packing, restricts segmental motion, and thus increases T_g. Although extensive studies explored these individual anions in PIL-based ion gels, a comprehensive understanding of their combined effects in mixed-anion systems remains limited. A remarkable feature of ion gels lies in the vast combinatorial landscape of cation–anion pairs. This chemical diversity holds great potential for tailoring gel properties for specific applications. However, such diversity also presents a challenge: a fundamental, structure–property understanding of how anion size and electrostatic interactions govern the behavior of ILs and PILs is still lacking. Addressing this gap is crucial for rationally designing high-performance ion gels.

In this study, we systematically investigate the effects of different anion combinations on the mechanical properties and ionic conductivity of PIL-based ion gels (**Scheme 1**). To this end, we elucidate the role of anion exchange and its influence on final gel properties by preparing gels with PILs bearing either TFSI or PF_6 anions, paired with ILs containing corresponding or mixed anions. Through rheological analysis, uniaxial tensile testing, and impedance spectroscopy, we provide insights into how the anion composition governs both mechanical toughness and ion transport functionality. Our findings establish a strategic framework for tuning PIL-based ion gels by manipulating anion identity, paving the way for their use in flexible electronics, energy storage, and soft robotics.

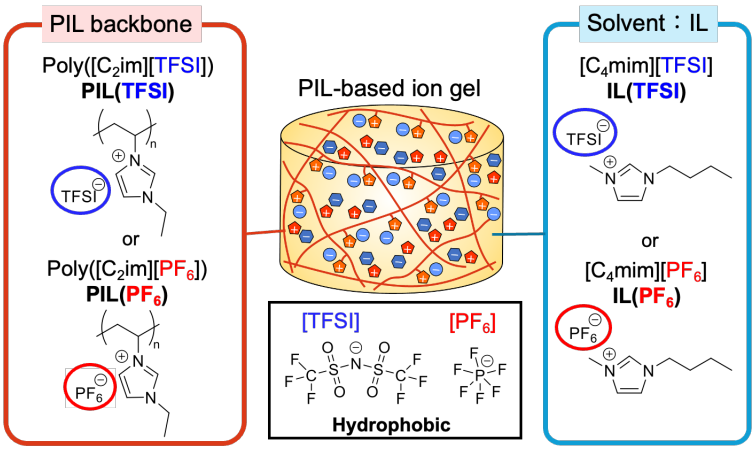

Scheme 1. Composition of PIL-based ion gels used in this study.

2. MATERIALS AND METHODS

2.1. Materials

An IL 1-butyl-3-methylimidazolium bis(trifluoromethanesulfonyl)imide ([C_4mim][TFSI]), an IL monomer 1-ethyl-3-vinylimidazolium bis(trifluoromethanesulfonyl)imide ([C_2vim][TFSI]), 1-vinylimidazole, 1,4-dibromobutane, ethanol, ethyl acetate (EA), diethyl ether, and lithium bis(trifluoromethanesulfonyl)imide (LiTFSI) were purchased from FUJIFILM Wako Pure Chemical Corporation (Osaka, Japan) and used as received. Potassium hexafluorophosphate (KPF_6) and hexafluorobenzene (C_6F_6) were obtained from TCI (Tokyo, Japan) and used as received. In addition, 2-hydroxy-4'-(2-hydroxyethyl)-2-methylpropiophenone (Ciba® IRGACURE® 2959) purchased from Ciba Specialty Chemicals (Switzerland) was used as a photoinitiator to synthesize the PIL network in ILs. The IL 1-butyl-3-methylimidazolium hexafluorophosphate ([C_4mim][PF_6]) and dimethyl sulfoxide-d_6 (DMSO-d_6) were purchased from Sigma-Aldrich (Japan) and used as received. The deionized water used in all experiments was produced using an Elix UV purification system (Millipore, Japan). **Figure S1** shows the chemical structures of [C_4mim][TFSI], [C_4mim][PF_6], [C_2vim][TFSI], [C_2vim][PF_6], Ciba® IRGACURE® 2959, [$(Vim)_2C_4$]Br_2, [$(Vim)_2C_4$][TFSI]$_2$, and [$(Vim)_2C_4$][PF_6]$_2$.

2.2. NMR measurements

The structures of synthesized IL monomers and crosslinkers were confirmed by ^{1}H NMR and ^{19}F NMR spectroscopy using a JNM-ECZL400S spectrometer (JEOL, Japan). ^{1}H NMR measurements were referenced to residual solvent signals (DMSO-d_6) (δ = 2.5 ppm), and ^{19}F NMR spectra were referenced to C_6F_6 (δ = −164.9 ppm) as the internal standard.

2.3. Synthesis of $[(Vim)_2C_4][TFSI]_2$ as a cross-linking reagent containing IL groups

The cross-linking reagent $[(Vim)_2C_4][TFSI]_2$ containing IL groups was synthesized by reacting 1-vinylimidazole with 1,4-dibromobutane, followed by an anion exchange reaction with LiTFSI (**Scheme S1**). 1-vinylimidazole (0.20 mol, 18.1 mL) was dissolved in ethanol (15.0 mL) in a 300-mL round-bottom flask, dried, and purged with argon. Subsequently, 1,4-dibromobutane (0.11 mol, 13.6 mL) was added dropwise to the flask, and the mixture was stirred at 70 °C under an argon atmosphere for 24 h. The reaction mixture was precipitated thrice in EA (300 mL) to remove unreacted reagents. The purified product was dried at 50 °C under reduced pressure overnight to obtain $[(Vim)_2C_4]Br_2$ (30.2 g, yield: 75% according to the ^{1}H NMR spectrum shown in **Figure S2a**[28]. Then, the anion exchange reaction of $[(Vim)_2C_4]Br_2$ with LiTFSI was performed by mixing an aqueous solution (60 mL) containing $[(Vim)_2C_4]Br_2$ (7.4 mmol, 3.00 g) with another aqueous solution (60 mL) containing LiTFSI (16.5 mmol, 4.73 g). The resulting mixture was stirred at 25 °C for 24 h under an argon atmosphere to exchange the Br_2 counter anion with $[TFSI]_2$ anions. The resulting $[(Vim)_2C_4][TFSI]_2$ was washed thrice with pure water (100 mL) and freeze dried for 24 h to remove any residual salt and obtain $[(Vim)_2C_4][TFSI]_2$ (4.7 g, yield: 78.5% according to the ^{1}H NMR spectrum in **Figure S2b**. The successful anion exchange from Br to TFSI was confirmed by the shift in peak from a' (9.59 ppm, 2H in **Figure S2a**) to a (9.42 ppm, 2H in **Figure S2b**) and the presence of a peak at –79.0 ppm on ^{19}F NMR spectra (**Figure S3**)[29].

2.4. Synthesis of $[(Vim)_2C_4][PF_6]_2$ as a cross-linking reagent containing ionic liquid groups

The anion exchange reaction of $[(Vim)_2C_4]Br_2$ with KPF_6 was performed by mixing an aqueous solution (60 mL)

containing $[(Vim)_2C_4]Br_2$ (7.4 mmol, 3.00 g) with another aqueous solution (60 mL) containing KPF_6 (16.6 mmol, 3.06 g) to synthesize $[(Vim)_2C_4][PF_6]_2$ (**Scheme S2**). The resulting mixture was stirred at 25 °C for 24 h under an argon atmosphere to exchange the Br counter anion with the PF_6 anion. The resulting $[(Vim)_2C_4][PF_6]_2$ was washed five times with pure water (100 mL) and freeze dried for 24 h to remove any residual salt and obtain $[(Vim)_2C_4][PF_6]_2$ (1.75 g, yield: 44.1% according to the ^{1}H NMR spectrum in **Figure S4**). The successful anion exchange from Br to PF_6 was confirmed by the shift in peak from a (9.59 ppm, 2H in **Figure S4a**) to a' (9.44 ppm, 2H in **Figure S4b**). In addition, the ^{19}F NMR spectrum obtained after the anion exchange reaction showed a doublet at –69.5 and –71.4 ppm, which indicated the successful synthesis of $[(Vim)_2C_4][PF_6]_2$ (**Figure S5**).

2.5. Synthesis of $[C_2vim][PF_6]$ as a monomer containing ionic liquid group

The IL monomer $[C_2vim][PF_6]$ was synthesized by reacting 1-vinylimidazole with bromobutane followed by an anion exchange reaction with KPF_6 (**Scheme S3**). 1-Vinylimidazole (75 mmol, 6.8 mL) was dissolved in ethanol (8 mL) in a 300-mL three-neck round-bottom flask that was dried and purged with argon. Subsequently, bromobutane (113 mmol, 8.4 mL) was added dropwise to the flask, and the mixture was stirred at 50 °C under an argon atmosphere for 4 days. After the reaction, ethanol and the remaining bromoethane were removed by a rotary evaporator. Then, the purified product was dried at 60 °C under reduced pressure overnight to obtain $[C_2vim][Br]$ (14.7 g, yield: 72.1%, according to ^{1}H NMR spectrum in **Figure S6**). The anion exchange reaction of $[C_2vim][Br]$ with KPF_6 was performed by mixing an aqueous solution (70 mL) containing $[C_2vim][Br]$ (49 mmol, 9.97 g) with KPF_6 (90 mmol, 16.6 g). The resulting mixture was stirred at 25 °C for 4 days under an argon atmosphere to exchange the Br counter anion with the PF_6 anion. The crude $[C_2vim][PF_6]$ was washed five times with pure water (20 mL) and dried at 70 °C under reduced pressure for 6 h to obtain $[C_2vim][PF_6]$ (5.3 g, yield: 40.5%). The successful anion exchange from Br to PF_6 was confirmed by the shift in peak from a' (9.60 ppm, H in **Figure S7a**) to a (9.45 ppm, H in **Figure S7b**). Further, the ^{19}F NMR spectrum after the anion exchange reaction showed a doublet at –69.5 and –71.4 ppm, indicating the successful synthesis of

$[C_2vim][PF_6]$ (**Figure S8**)[30].

2.6. Preparation of PIL-based ion gels

PIL-based ion gels with different anion combinations were prepared via the photopolymerization of an IL monomer in the presence of IL and EA as a cosolvent. The cosolvent serves to reduce the viscosity of mixtures and enhance the solubility of the initiator. The polymer network was crosslinked using a divinylimidazolium-based crosslinking agent. The IL monomer ($[C_2vim][TFSI]$ or/and $[C_2vim][PF_6]$) (1.5 g) was mixed with a crosslinking agent ($[(Vim)_2C_4][TFSI]_2$ or/and $[(Vim)_2C_4][PF_6]_2$) (0.015 g) along with the photoinitiator IRGACURE® 2959 (0.8 mg), ILs ($[C_4mim][TFSI]$, or/and $[C_4mim][PF_6]$) (1.7 g), and EA (1.0 mL). The mixture was homogenized using a vortex mixer followed by stirring to obtain the precursor solution, and then, the solution was injected into a mold comprising two glass plates with a Fluorinated Ethylene Propylene film and a 1-mm-thick Polytetrafluoroethylene spacer. The polymerization was conducted under ultraviolet (UV) irradiation (365 nm) for 17 h (1,820 $\mu W/cm^2$). After polymerization, the ion gel was dried under vacuum at 40 °C for 3 h for removing the residual EA. The amounts of reagent are summarized in **Table S1**–**S5**. It is noted that due to the high T_g and resultant brittleness of PIL(PF_6)/IL(PF_6) ion gels at IL contents below 50 wt%, these samples were difficult to mold and characterize reproducibly. Therefore, the IL content range for PF_6 was restricted to 50–80 wt% (**Table S5**), in contrast to the 10–70 wt% range used for PIL(TFSI)/IL(TFSI) ion gels (**Table S4**).

2.7. Rheological measurements

Oscillatory shear measurements were performed with an Anton Paar MCR 302 rheometer (Anton Paar, Austria) using a parallel-plate geometry with a 25-mm-diameter plate (PP25). The gap spacing was set to 0.5 mm for all measurements, and frequency sweep measurements were performed over a frequency range of 0.01–100 Hz with a strain amplitude of 0.1% at constant temperatures from –40 to 180 °C at intervals of 10 °C. For each 10 °C increment, the sample was

equilibrated for 10 min before data acquisition. The time-temperature superposition (tTS) master curves for the gels were constructed from the frequency sweep data at different temperatures.

Temperature-sweep measurements of ion gels were performed with a parallel-plate geometry (PP25; diameter = 25 mm) using the same rheometer. The measurement parameters included a normal force, temperature range, frequency, and strain of 4 N, −100–200 °C, 1 Hz, and 0.1%, respectively. Further, T_g was determined as the temperature at the peak top of tan δ.

2.8. Tensile tests

Mechanical properties of ion gels were evaluated using an automatic recording universal testing instrument (EZ Test EZ-SX 500 N, Shimadzu Corporation, Japan) at 25 °C. Dumbbell-shaped specimens with lengths, widths, and thicknesses of 35, 2, and 1 mm, respectively, were used for the tensile tests. The fabricated samples were attached to the instrument. The distance between the jigs was fixed at 15 mm. The uniaxial stretching test was performed by stretching the sample at a constant strain rate of 50 mm/min. The stress–strain curves were recorded automatically until the specimens broke. The fracture stresses, strains, and energies in addition to the Young's moduli of the ion gels were obtained as mean values of the triplicate measurements conducted for each sample.

2.9. SEM-EDX analysis

The ion gel was cut into square pieces (5–10 mm per side) and immersed in an excess amount of acetone (500 times the mass of the gel) to induce swelling. After the ion gel was allowed to swell for one day, the external liquid was removed, and the gel was re-immersed in fresh acetone. This procedure was repeated more than ten times to remove the incorporated IL. Subsequently, the gel was naturally dried under a fume hood, followed by vacuum drying. A dried PIL elastomer was subjected to SEM-EDX analysis to quantify its elemental composition. Based on the weight change before and after immersion, the anion exchange ratio was calculated under the assumption that the initial monomer

incorporation rate was 100%.

2.10. Ionic conductivity measurements

Ionic conductivity values of gel films were measured by the impedance analyzer using an LCR meter (IM3536, Hioki, Japan) in the frequency range of 4 Hz–10 MHz in the temperature range of −20–120 (above the T_g of each sample). The sample was sandwiched between two copper plates, and the ionic conductivity (σ [mS/cm]) was evaluated using the formula $\sigma = L/(R \times A)$, where L is the thickness of the sample, R is the bulk resistance, and A is the contact area between the two copper plates.

3. RESULTS AND DISCUSSION

3.1. Effect of Combining PIL and IL Anion on the Mechanical Properties of Ion Gels

To evaluate the effect of different anion species on the mechanical properties and viscoelastic behaviors of ion gels, we first prepared four types of gels via the photopolymerization of IL monomers ([C_2vim][TFSI] or [C_2vim][PF_6]) in mixtures containing IL ([C_4mim][TFSI] (IL-TFSI) or [C_4mim][PF_6] (IL-PF_6)), a photoinitiator (IRGACURE 2959), a cross-linker ([$(Vim)_2C_4$][$TFSI]_2$ or [$(Vim)_2C_4$][$PF_6]_2$), and EA as a cosolvent. After polymerization, EA was subsequently removed via evaporation to yield ion gels with the following PIL/IL combinations: PIL(TFSI)-50wt/IL(TFSI)-50wt, PIL(TFSI)-50wt/IL(PF_6)-50wt, PIL(PF_6)-50wt/IL(TFSI)-50wt, and PIL(PF_6)-50wt/IL(PF_6)-50wt. The IL content in all samples was fixed at 53 wt%. The details are summarized in **Table 1**.

Table 1. Compositions of PIL-based ion gels with varying anion species.

Entry	Monomer	IL	Cross-linker	IL content		ϕ_{PF6} =[PF_6]/([TFSI]+[PF_6])
			[mol%]*1	[wt%]*2	[mol%]	[-]
Entry 1	PIL(TFSI)-50wt/IL(TFSI)-50wt	[C_2vim][TFSI]	[C_4mim][TFSI]	0.50	53	52	0
Entry 2	PIL(TFSI)-50wt/IL(PF_6)-50wt	[C_2vim][TFSI]	[C_4mim][PF_6]	0.50	53	62	0.61
Entry 3	PIL(PF_6)-50wt/IL(TFSI)-50wt	[C_2vim][PF_6]	[C_4mim][TFSI]	0.50	53	42	0.58
Entry 4	PIL(PF_6)-50wt/IL(PF_6)-50wt	[C_2vim][PF_6]	[C_4mim][PF_6]	0.50	53	52	1.0
Entry 5	PIL(TFSI)-50mol/IL(PF_6)-50mol	[C_2vim][TFSI]	[C_4mim][PF_6]	0.50	41	50	0.50
Entry 6	PIL(PF_6)-50mol/IL(TFSI)-50mol	[C_2vim][PF_6]	[C_4mim][TFSI]	0.50	61	50	0.50
Entry 7	PIL(TFSI)/IL(TFSI)-0	[C_2vim][TFSI]	[C_4mim][TFSI]	0.50	53	52	0
Entry 8	PIL(PF_6/TFSI)/IL(PF_6/TFSI)-0.25	[C_2vim][TFSI] +[C_2vim][PF_6]	[C_4mim][TFSI] +[C_4mim][PF_6]	0.50	53	52	0.25
Entry 9	PIL(PF_6/TFSI)/IL(PF_6/TFSI)-0.50	[C_2vim][TFSI] +[C_2vim][PF_6]	[C_4mim][TFSI] +[C_4mim][PF_6]	0.50	54	53	0.50
Entry 10	PIL(PF_6/TFSI)/IL(PF_6/TFSI)-0.75	[C_2vim][TFSI] +[C_2vim][PF_6]	[C_4mim][TFSI] +[C_4mim][PF_6]	0.50	54	53	0.75
Entry 11	PIL(PF_6)/IL(PF_6)-1.0	[C_2vim][PF_6]	[C_4mim][PF_6]	0.50	53	52	1.0

*1 Initiator concentration was fixed at 0.1 wt% against the monomer amount. *2 IL weight concentration in the gel.

Figure 1 shows images of ion gels, all of which exhibited high optical transparency without phase separation, regardless of the PIL and IL combinations. This observation indicates that PILs and ILs containing either TFSI or PF_6 anions have high mutual compatibility. Stress–strain curves obtained from uniaxial tensile tests (**Figure 2a** and **2b**) reveal that ion gels containing PF_6 anions exhibited higher mechanical strength compared to those containing TFSI anions. Among mixed-anion conditions, the PIL(PF_6)-50wt/IL(TFSI)-50wt exhibited higher mechanical strength than that of the PIL(TFSI)-50wt/IL(PF_6)-50wt ion gel. The PIL(PF_6)-50wt/IL(PF_6)-50wt sample was the only one that

exhibited a distinct yield point and high Young's modulus (**Figure 2c**), thereby suggesting superior mechanical robustness.

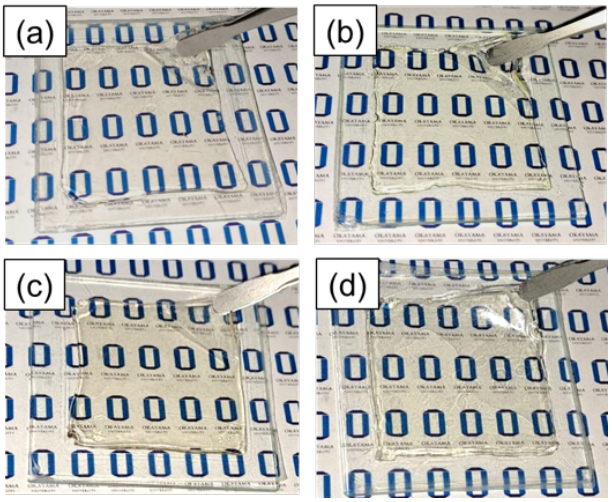

Figure 1. Photographs of PIL ion gels with different anion combinations: **(a)** PIL(TFSI)-50wt/IL(TFSI)-50wt, **(b)** PIL(TFSI)-50wt/IL(PF_6)-50wt, **(c)** PIL(PF_6)-50wt/IL(TFSI)-50wt, and **(d)** PIL(PF_6)-50wt/IL(PF_6)-50wt.

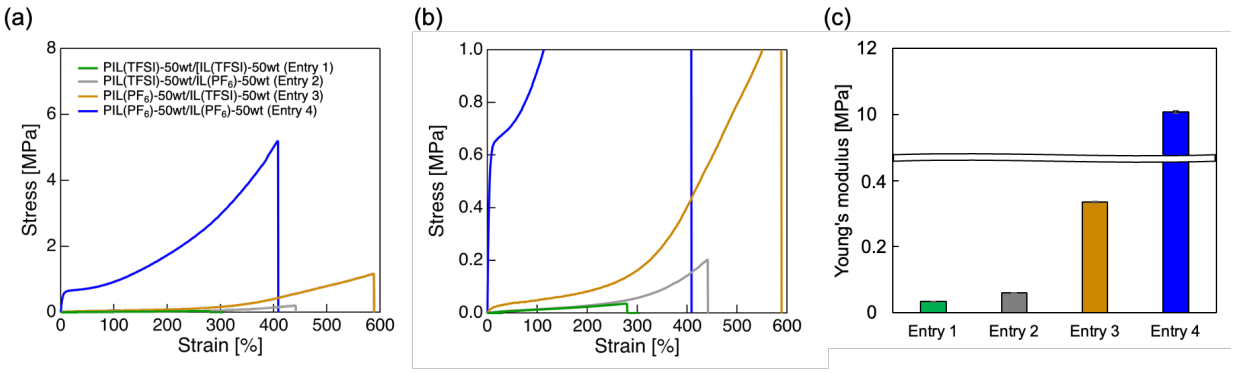

Figure 2. (a) Overview of stress–strain curves and **(b)** magnified view of stress–strain curves of PIL ion gels with different anion combinations. **(c)** Young's modulus of PIL ion gels corresponding to each anion combination.

Figure 3 represents time-temperature superposition (tTS) master-curves constructed using a shift factor (a_T) based on the tTS principle. This approach characterizes viscoelastic properties over a broad time or frequency range by performing frequency sweep measurements at various temperatures. Inset values in Figure 3 indicate measurement temperatures, with 20 °C used as the reference temperature (T_{ref}). Good superposition of the curves was achieved under

all conditions across the tested temperature range. The T_g was estimated from the peak temperature of tanδ (= G''/G'), which yields –20, 10, 20, and 70 °C for the PIL(TFSI)-50wt/IL(TFSI)-50wt, PIL(TFSI)-50wt/IL(PF_6)-50wt, PIL(PF_6)-50wt/IL(TFSI)-50wt, and PIL(PF_6)-50wt/IL(PF_6)-50wt, respectively (**Figure S9**). In the rubbery plateau region, the storage modulus *G*' is nearly frequency-independent, and its magnitude (G_0) reflects the density of elastically effective network strands. To elucidate the network structure of the ion gels, the effective cross-link density ν_e[/m^3] was estimated using the relation $\nu_e = \frac{G_0}{k_B T}$, where G_0 is the plateau modulus [Pa], k_B is the Boltzmann constant [J/K], and T is the absolute temperature [K] corresponding to the plateau region. As summarized in **Table S6**, the calculated ν_e values increased systematically with PF_6 content. Importantly, the crosslinker concentration was fixed at 0.5 mol% across all samples, indicating that this increase in ν_e would not originate from differences in covalent crosslinking density. We attribute this to the effects of the anion species: the smaller size and stronger electrostatic interactions of PF_6 with polymer chains enhance polymer chain packing and ionic association, thereby promoting the formation of a denser network structure. These findings emphasize the critical role of anion species in determining both the stiffness and the efficiency of network formation.

The superior mechanical properties observed in PF_6-containing ion gels can be attributed to smaller anion size, which promotes denser packing and reduced segmental mobility, leading to their higher T_g values. The distinct yield point and high Young's modulus of PIL(PF_6)-50wt/IL(PF_6)-50wt is due to its T_g exceeding the measurement temperature (20 °C), which restricts polymer chain mobility under tensile test conditions. To support this interpretation, the Weissenberg number (W_i) was calculated based on the segmental relaxation time (τ) and the strain rate (γ), as summarized in **Table S7**. Notably, PIL(PF_6)-50wt/IL(PF_6)-50wt gels only exhibited $W_i > 1$, suggesting insufficient relaxation during deformation and resulting in a more elastic response with yield point. In contrast, the other gels exhibited $W_i \ll 1$, indicating that polymer chains could sufficiently relax under tensile loading.

Differences in T_g and mechanical strength between the mixed-anion systems (PIL(TFSI)-50wt/IL(PF_6)-50wt vs. PIL(PF_6)-50wt/IL(TFSI)-50wt) can be explained by the difference in IL molar concentration. Since the IL content

was fixed by weight, the PIL molar concentration was higher in PIL(PF_6)-50wt/IL(TFSI)-50wt than that in PIL(TFSI)-50wt/IL(PF_6)-50wt, resulting in a more robust gel network.

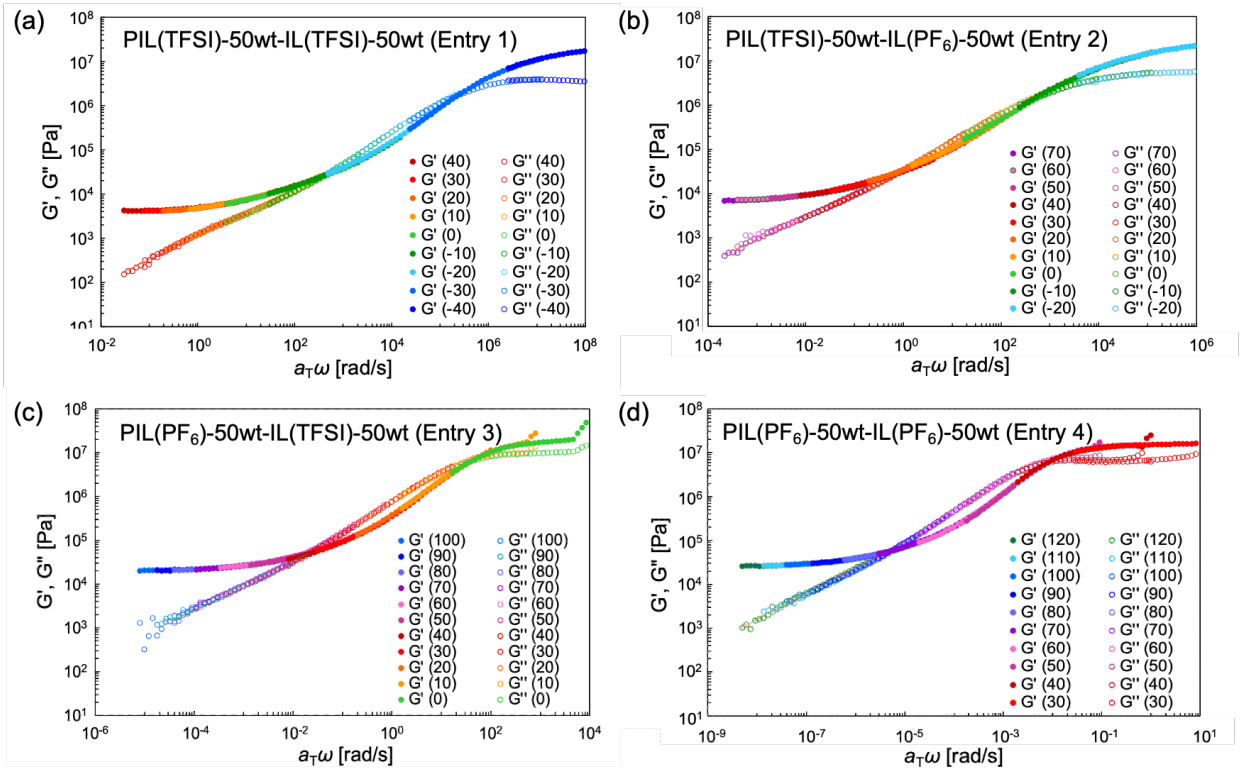

Figure 3. tTS master-curves of PIL-based ion gels with different anion combinations: **(a)** PIL(TFSI)-50wt/IL(TFSI)-50wt, **(b)** PIL(TFSI)-50wt/IL(PF_6)-50wt, **(c)** PIL(PF_6)-50wt/IL(TFSI)-50wt, and **(d)** PIL(PF_6)-50wt/IL(PF_6)-50wt. The T_{ref} value is 20 °C.

Physical Property Evaluation of PIL-based Ion Gels with an Equal Molar Ratio of TFSI and PF_6 Anions

As detailed shown in **Figure S10** and **S11**, elemental analysis via SEM-EDX revealed substantial anion exchange between the PIL network and the IL component during gel formulation, resulting in a final anion composition that differs markedly from the starting feed ratio. This spontaneous anion exchange suggests that dynamic ion partitioning is governed by the molar ratio of IL monomer and IL during gelation. To further investigate how the overall anion

composition influences the physical properties of the ion gels, we prepared PIL-based ion gels with IL concentrations fixed at 50 mol% and an equimolar ratio of TFSI and PF_6 anions in gels: PIL(TFSI)-50mol/IL(PF_6)-50mol ion gel and PIL(PF_6)-50mol/IL(TFSI)-50mol ion gel (**Table 1**) and evaluated their mechanical and viscoelastic behaviors.

Figure 4a represents the stress–strain curves of these ion gels, which confirm that both gels exhibited similar mechanical properties. The measured T_g values were −22 °C for PIL(TFSI)-50mol/IL(PF_6)-50mol and −25 °C for PIL(PF_6)-50mol/IL(TFSI)-50mol, which demonstrated that there was no significant difference in T_g between them (**Figure S12**). Further, the tTS master curves of both samples overlapped, suggesting that anion exchange between PIL and IL during preparation resulted in similar structural characteristics (**Figure 4b**). These results confirmed that the properties of PIL-based ion gels could be effectively tuned by controlling the overall anion composition within the gel system.

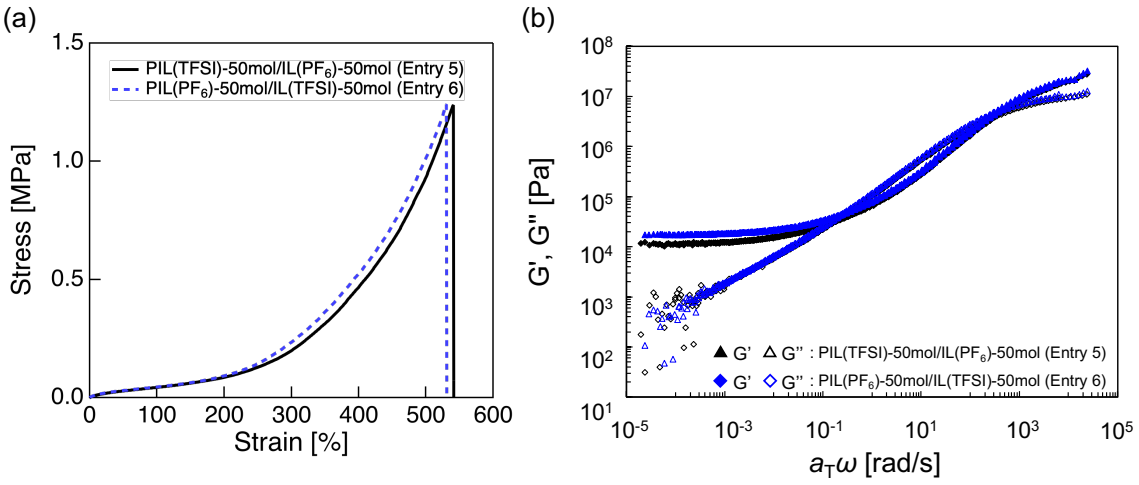

Figure 4. (a) Stress–strain curves and **(b)** tTS master curves of PIL ion gels with different combination of anions and same IL molar concentration. Entry 5: PIL(TFSI)-50mol/IL(PF_6)-50mol ion gels, Entry 6: PIL(PF_6)-50mol/IL(TFSI)-50mol ion gel.

Effect of the Mixing Ratio of PF_6 to TFSI Anions in PIL-based Ion Gels on Their Properties

We found that the ratio of PF_6 to TFSI anions in PIL-based ion gels significantly influences their mechanical and electrochemical properties. Importantly, this effect arises from the overall anion composition, regardless of whether the anions originate from the PIL or the IL component. To investigate this systematically, five types of PIL-based ion gels were prepared with varying anion compositions, defined by the molar fraction of PF_6 as ϕ_{PF6} = [PF_6]/([TFSI]+[PF_6]) [-] = 0, 0.25, 0.50, 0.75, and 1.0 (**Table 1**). **Figure 5a** illustrates the dependence of T_g on the PF_6 content. T_g increases monotonically with increasing PF_6 content, which can be attributed to the smaller ionic radius of PF_6 compared to that of TFSI. This size difference leads to a reduction in free volume and enhanced packing density within the network. **Figure 5b** represents the stress–strain curves obtained from tensile tests. A clear increase in fracture strain, fracture stress, fracture energy, and Young's modulus was observed with an increasing PF_6 content. The gel containing only PF_6 anions (ϕ_{PF6} = 1.0) exhibited the highest Young's modulus. The increase in T_g restricts chain mobility at room temperature, resulting in a stiffer and more glassy behavior under uniaxial deformation.

The ionic conductivity (σ) of the PIL-based ion gels was measured using an impedance analyzer, plotted with an inverted temperature (**Figure 5c**), and fitted with the Vogelvalues–Fulcher–Tammann (VFT) equation (1):

$$\sigma = \sigma_0 exp\,[-B/(T - T_0)] \qquad (1)$$

where σ_0, B, and T_0 represent the ionic conductivity at infinite temperature, pseudo activation energy for ionic conduction, and Vogel temperature, respectively. The fitting parameters are summarized in **Table S8**. It should be noted that the VFT fitting in this study was primarily used as a comparative tool to assess relative trends across different samples, rather than to derive absolute physical parameters. The B parameter is thus treated as a pseudo activation energy and is not intended to be interpreted as a true activation energy.

The increasing trend in the pseudo activation parameter B with PF_6 content indicates reduced ion mobility due to stronger ion–ion interactions and increased network rigidity. Consequently, σ decreases with increasing PF_6 concentration, highlighting the dominant role of restricted segmental dynamics over thermal activation. These findings suggest that the larger ionic radius of TFSI compared to that of PF_6 leads to weaker electrostatic interactions and easier

dissociation from cations, thereby facilitating ion transport over T_g. To normalize for thermal behavior, conductivity was also plotted against the reduced temperature (T/T_g) in **Figure 5d**. While the σ values converged at higher T/T_g, notable differences emerged near $T/T_g \approx 1$. In this regime, conductivity increased with higher PF_6 content. This behavior suggests that ion transport near T_g is not governed solely by thermal activation, but is significantly affected by anion species, ion concentration, and network density due to restricted segmental motion. It should be noted that T_g values obtained from the peak of tan δ likely overestimate the actual onset of restricted chain mobility. This discrepancy may partially explain the relatively high σ values observed near T_g in our system. As previously reported by Choi et al.[31], ionic conductivity near T_g is predominantly determined by the available free ion concentration rather than their mobility. Our results are consistent with this framework and suggest a universal trend across PIL-based ion materials.

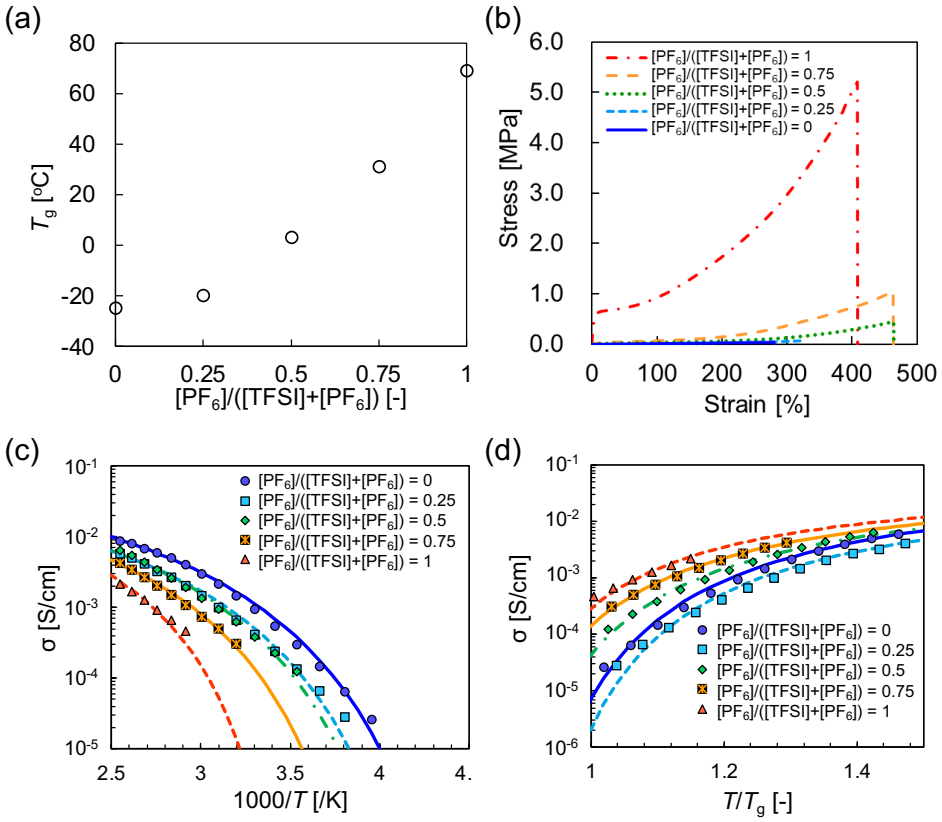

Figure 5. Properties of PIL-based ion gels with different $[PF_6]/([TFSI]+[PF_6])$. **(a)** T_g, **(b)** Stress–strain curves, **(c)** Ion conductivities as a function of inverse temperature, and **(d)** ion conductivity as a function of normalized temperature (T/T_g).

There are two possible key factors that contribute to the enhanced ionic conductivity observed in PF_6-rich ion gels: the ion number density and the ease of anion hopping. First, regarding ion number density (p_0) [ions/cm^3], this parameter represents the total number of charge carriers in the gel, which is calculated using the following equation (2):

$$p_0 = \frac{\rho_0 N_A}{M_w} \qquad (2)$$

where ρ_0 is the ion gel density [g/cm^3], N_A is Avogadro's number [1/mol], and M_w is the Average molecular weight of the ion gel [g/mol]. The resulting ion number densities were 2.2×10^{21} [ions/cm^3] for the gel containing only TFSI anions ($\phi_{PF6} = 0$) and 3.1×10^{21} [ions/cm^3] for the sample containing only PF_6 anions ($\phi_{PF6} = 1.0$). This indicates that the sample containing only PF_6 showed a 1.5 times higher ion number density than that containing only TFSI. Second, the mobility of anions, particularly under suppressed thermal motion near T_g, ion transport is widely believed to occur predominantly via ion hopping mechanism[32]. In this case, the smaller size and higher mobility of PF_6 anions likely facilitate more efficient hopping transport compared to the bulky TFSI anions. These factors could contribute to the enhanced ionic conductivity observed in PF_6-rich ion gels. However, we also recognize that these explanations would not fully explain the conductivity differences observed across the samples. Thus, further study will be needed to clarify the detailed molecular mechanisms, particularly near T_g. These results nonetheless confirm that adjusting the mixing ratio of PF_6 to TFSI in PIL-based ion gels offers a rational and versatile approach to simultaneously control mechanical properties and ionic conductivity. These findings provide valuable insights for designing ion gels tailored for electrochemical and soft-matter applications.

Effects of IL concentration on the properties of PIL-based ion gels

We investigated the effect of IL concentration on the thermal, mechanical, and electrochemical properties of PIL-based ion gels, using either TFSI or PF_6 as a fixed anion. For both systems, T_g decreased systematically with increasing IL

content due to the plasticizing effect of ILs (**Figure S13**). As the IL content increased, the relative concentration of PIL in the gel decreased, weakening the network structure and resulting in reduced mechanical strength. This trend is clearly demonstrated by the decrease in fracture strain, fracture stress, fracture energy, and Young's modulus, as shown in **Figure 6a and b,** and **Figure S14**.

Figure S15 shows the relationship between T_g and the mechanical properties such as fracture strain, fracture stress, fracture energy, and Young's modulus. A good correlation between T_g and mechanical strength was observed in all cases, but complete convergence was not confirmed. This suggests that mechanical properties are governed not only by T_g itself, but also by molecular-level interactions that differ with the anion species, as we discussed above.

Ionic conductivity (σ) increased with higher IL concentrations (**Figure 6c and d**), which is due to plasticizing effect and the associated increase in ion mobility. **Table S9** presents the fitting parameters derived from the VFT equation. The B values for ionic conduction showed a decrease trend with increasing IL content, which suggest that enhanced segmental motion with decreasing T_g facilitates ion transport.

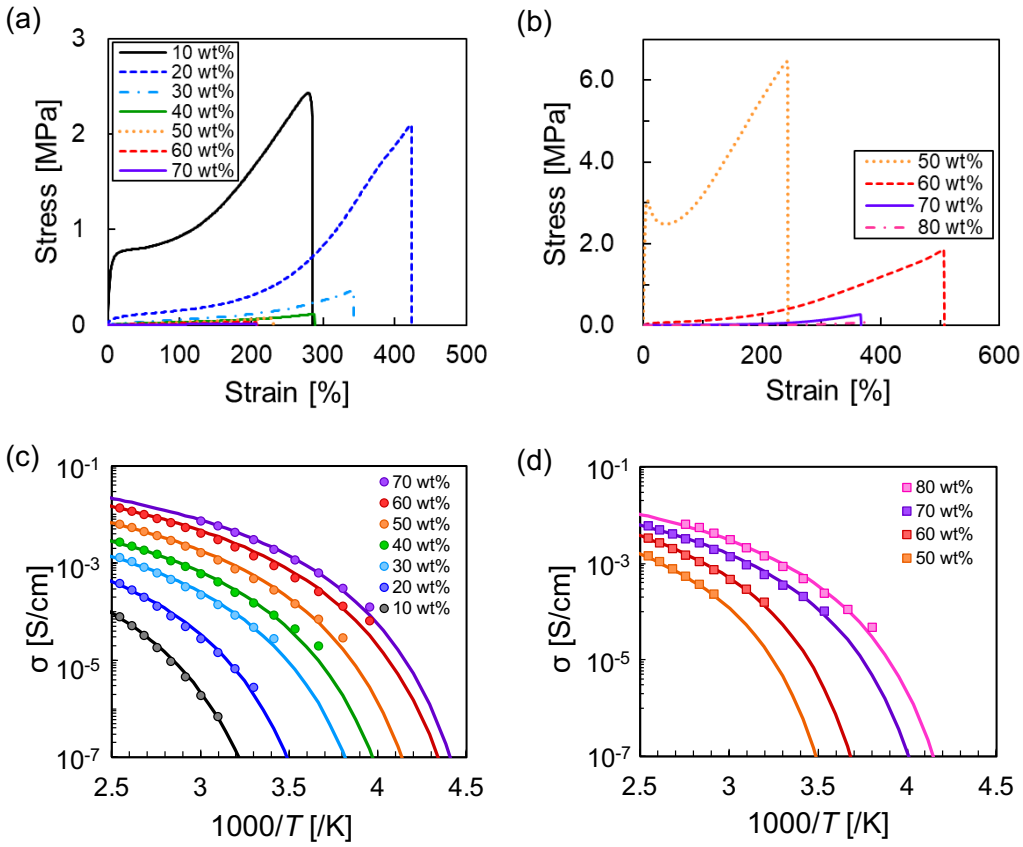

Figure 6. Stress–strain curves and ionic conductivity of PIL ion gels with different IL concentrations **(a** and **c)** PIL(TFSI)/IL(TFSI) ion gels, and **(b** and **d)** PIL(PF_6)/IL(PF_6) ion gels.

CONCLUSIONS

In this study, we systematically investigated the effect of anion composition and IL concentration on the mechanical properties and ionic conductivity of PIL-based ion gels. Our results demonstrated that the selection and mixing ratio of anions (TFSI and PF_6) play crucial roles in determining the mechanical strength, viscoelastic behavior, and ionic conductivity of the gels. PF_6-rich ion gels exhibited enhanced mechanical robustness, which we attribute to the smaller size of the PF_6 anion that promotes stronger electrostatic interactions with the cationic polymer segments and leads to denser polymer chain packing. These factors increase the apparent crosslinking density and restrict chain mobility, resulting in a higher glass transition temperature (T_g) and greater mechanical stiffness. In contrast, TFSI-rich ion gels showed higher ionic conductivity due to their larger anion size, weaker electrostatic interactions, and looser polymer packing, which reduces apparent crosslinking density and increases free volume, thereby lowering T_g and enhancing ion mobility. Interestingly, near T_g, PF_6-rich ion gels exhibited higher ionic conductivity than TFSI-rich ion gels, likely due to an increased density of mobile ions and more efficient ion hopping associated with the smaller PF_6 anion. Furthermore, anion exchange between the PIL network and IL solvent was confirmed, which suggested that the final anion composition, instead of the specific source of anions (PIL or IL), dictates the gel properties. We demonstrated that controlling the overall anion composition provides a direct means of tuning gel properties by preparing gels with an equal molar ratio of TFSI and PF_6 anions. In addition, IL concentration was found to strongly influence both mechanical strength and ionic conductivity; a higher IL content led to reduced mechanical strength because of plasticization but improved ionic conductivity by enhancing ion mobility. Despite these findings, several limitations remain. The study focused on only two common anions (TFSI and PF_6), and further investigations are required to explore the effects of other anions with different steric and electronic properties. In addition, our study examined bulk mechanical and conductive properties; however, localized heterogeneities and long-term stability under practical conditions remain open questions.

ASSOCIATED CONTENT

SUPPORTING INFORMATION

Supporting Information is available free of charge on the ACS Publications website at DOI:xxx.

Chemical structures of reagents used to prepare PIL ion gels; Synthesis of $[(Vim)_2C_4]Br_2$ and $[(Vim)_2C_4]$ $[TFSI]_2$; ^1H NMR spectra of $[(Vim)_2C_4]Br_2$ and $[(Vim)_2C_4]$ $[TFSI]_2$; ^{19}F NMR spectra of $[(Vim)_2C_4]Br_2$ and $[(Vim)_2C_4]$ $[TFSI]_2$.; Synthesis of $[(Vim)_2C_4]$ $[PF_6]_2$, ^1H NMR spectra of $[(Vim)_2C_4]Br_2$ and $[(Vim)_2C_4]$ $[PF_6]_2$; ^{19}F NMR spectra of $[(Vim)_2C_4]Br_2$ and $[(Vim)_2C_4]$ $[PF_6]_2$; Synthesis of $[C_2vim]Br$ and $[C_2vim][PF_6]$; ^1H NMR spectra (upper = 1-vinylimidazole, middle = bromoethane, bottom = $[C_2vim]Br$); ^1H NMR spectra of $[C_2vim]Br$ and $[C_2vim][PF_6]$. Solvent: DMSO-d_6); ^{19}F NMR spectra of $[C_2vim]Br$ and $[C_2vim][PF_6]$; Compositions of PIL-based ion gels with different anion combinations (Entry 1–4); Compositions of PIL-based ion gels with different anion combinations (Entry 5 and 6); Compositions of PIL-based ion gels with different anion combinations (Entry 7–11); Compositions of PIL(TFSI)/IL(TFSI) ion gels with different IL concentrations; Compositions of PIL(PF_6)/IL(PF_6) ion gels with different IL concentrations; Temperature-sweep measurements of PIL-based ion gels with different combination of anions; Effective cross-linking density of ion gels (Entry1–11); Weissenberg number (*Wi*) upon uniaxial tensile test for PIL-based ion gels with different anion combinations. *Wi* was calculated from the segmental relaxation time (τ) and the strain rate (γ); Evaluation of anion exchange between the PIL network and IL during preparation; SEM images of PIL elastomers prepared from Entry 2: PIL(TFSI)-50wt/IL(PF_6)-50wt ion gel and Entry 3: PIL(PF_6)-50wt/IL(TFSI)-50wt ion gel; Elemental maps of PIL elastomers measured by SEM-EDX measurement; Temperature-sweep measurements of PIL-based ion gels with different combination of anions and the same IL molar concentration; Temperature-sweep measurements of PIL-based ion gels with different combination of anions and the same IL molar concentration; VTF equation parameters for ionic conductivity data and glass transition temperatures for PIL ion gels with different ratio of anions (Entry7–11); Effect of IL content on the T_g value of PIL-based ion gels with different anion systems; Mechanical

properties of PIL ion gels with different IL concentrations. Fracture strain, fracture stress, fracture energy, and Young's modulus; Mechanical properties against the T_g value of PIL ion gels with different IL concentrations; Mechanical properties of PIL ion gels with different IL concentrations; VTF equation parameters for ionic conductivity data and glass transition temperatures for PIL ion gels with different IL concentrations.

AUTHOR INFORMATION

CORRESPONDING AUTHORS

Takaichi Watanabe − Department of Applied Chemistry, Graduate School of Environmental, Life, Natural Science, and Technology, Okayama University, 3-1-1, Tsushima-naka, Kita-ku, Okayama, 700-8530, Japan; orcid.org/0000-0002-5855-2583; Phone: +81-86-251-8072, E-mail: wata-t@okayama-u.ac.jp.

Tsutomu Ono − Department of Applied Chemistry, Graduate School of Environmental, Life, Natural Science, and Technology, Okayama University, 3-1-1, Tsushima-naka, Kita-ku, Okayama, 700-8530, Japan; orcid.org/0000-0002-2880-7119; Phone: +81-86-251-8083, E-mail: tono @okayama-u.ac.jp.

AUTHORS

Yuna Mizutani − Department of Applied Chemistry, Graduate School of Natural Science and Technology, Okayama University, 3-1-1, Tsushima-naka, Kita-ku, Okayama, 700-8530, Japan

Carlos G. Lopez − The Pennsylvania State University, 80 Pollock Rd, 16801 State College, US

ORCID

Takaichi Watanabe: 0000-0002-5855-2583

Yuna Mizutani: 0009-0006-1777-8144

Carlos G. Lopez: 0000-0001-6160-632X

Tsutomu Ono: 0000-0002-2880-7119

AUTHOR CONTRIBUTIONS

Y.M., T.W., and T.O. designed the experiments. T.W. and Y.M. performed the experiments and analyzed the data. Y.M., T.W., C.G.L., and T.O. interpreted the results and wrote the manuscript. T.W. designed the research.

ACKNOWLEDGEMENT

This work was partly supported by the JSPS KAKENHI (grant numbers: JP20KK0325 and JP21H04629), New Energy and Industrial Technology Development Organization (NEDO) (grant number: JPNP20004), and Young Faculty Promotion Program (2023) at Okayama University. We would like to express our sincere gratitude to the Japan Keirin Autorace Foundation (JKA) for their financial support (Grant No. 2024M-247).

NOTES

The authors declare no competing financial interest.

REFERENCES

(1) Wang, Y.; Chen, Y.; Gao, J.; Yoon, H. G.; Jin, L.; Forsyth, M.; Dingemans, T. J.; Madsen, L. A. Highly Conductive and Thermally Stable Ion Gels with Tunable Anisotropy and Modulus. *Adv. Mater.* **2016**, *28* (13), 2571–2578.

(2) Maton, C.; De Vos, N.; Stevens, C. V. Ionic Liquid Thermal Stabilities: Decomposition Mechanisms and Analysis Tools. *Chem. Soc. Rev.* **2013**, *42* (13), 5963–5977.

(3) Fox, D. M.; Gilman, J. W.; Morgan, A. B.; Shields, J. R.; Maupin, P. H.; Lyon, R. E.; De Long, H. C.; Trulove, P. C. Flammability and Thermal Analysis Characterization of Imidazolium-Based Ionic Liquids. *Ind. Eng. Chem. Res.* **2008**, *47* (16), 6327–6332.

(4) Lee, H.; Erwin, A.; Buxton, M. L.; Kim, M.; Stryutsky, A. V.; Shevchenko, V. V.; Sokolov, A. P.; Tsukruk, V. V. Shape Persistent, Highly Conductive Ionogels from Ionic Liquids Reinforced with Cellulose Nanocrystal Network. *Adv. Funct. Mater.* **2021**, *31* (38), 2103083.

(5) Zhao, G.; Lv, B.; Wang, H.; Yang, B.; Li, Z.; Junfang, R.; Gui, G.; Liu, W.; Yang, S.; Li, L. Ionogel-Based Flexible Stress and Strain Sensors. *Int. J. Smart Nano Mater.* **2021**, *12* (3), 307–336.

(6) Zhang, L. M.; He, Y.; Cheng, S.; Sheng, H.; Dai, K.; Zheng, W. J.; Wang, M. X.; Chen, Z. S.; Chen, Y. M.; Suo, Z. Self-Healing, Adhesive, and Highly Stretchable Ionogel as a Strain Sensor for Extremely Large Deformation. *Small* **2019**, *15* (21), e1804651.
(7) Sun, Y.; Cheng, Y.; Shi, L.; Sun, J.; Chen, S.; Wang, R. Dual Ion Regulated Eutectogels with High Elasticity and Adhesive Strength for Accurate Strain Sensors. *Adv. Funct. Mater.* **2024**, *34* (34), 2401808.
(8) Terasawa, N. Self-Standing High-Performance Transparent Actuator Based on Poly(Dimethylsiloxane)/TEMPO-Oxidized Cellulose Nanofibers/Ionic Liquid Gel. *Langmuir* **2020**, *36* (22), 6154–6159.
(9) Watanabe, M.; Imaizumi, S.; Yasuda, T.; Kokubo, H. Ion Gels for Ionic Polymer Actuators. In *Soft Actuators*; Springer Singapore: Singapore, 2019; pp 217–232.
(10) Ali, I.; Latif, A.; Hussain, K.; Shehzad, F. K.; Ali, A.; Faisal, R.; Xudong, L.; Dias, O. A. T.; Weimin, Y.; Haoyi, L. Ionic Liquids Enhanced Performance of PVC Gels Actuator. *J. Appl. Polym. Sci.* **2021**, *138* (29), 50710.
(11) Prasadini, K. W.; Perera, K. S.; Vidanapathirana, K. P. Preliminary Study on the Performance of a Redox Capacitor with the Use of Ionic Liquid-Based Gel Polymer Electrolyte and Polypyrrole Electrodes. *J. Mater. Sci.: Mater. Electron.* **2021**, *32* (13), 17629–17636.
(12) Yoshitake, M.; Han, J.; Sakai, T.; Morita, M.; Fujii, K. TetraPEG Network Formation via a Michael Addition Reaction in an Ionic Liquid: Application to Polymer Gel Electrolyte for Electric Double-Layer Capacitors. *Chem. Lett.* **2019**, *48* (7), 704–707.
(13) Lee, J. H.; Park, Y. S.; Cho, S.; Kang, I. S.; Kim, J. K.; Jeong, U. Output Voltage Modulation in Triboelectric Nanogenerator by Printed Ion Gel Capacitors. *Nano Energy* **2018**, *54*, 367–374.
(14) Zhang, J.; Kamio, E.; Matsuoka, A. Novel Tough Ion-Gel-Based CO2 Separation Membrane with Interpenetrating Polymer Network Composed of Semicrystalline and Cross-Linkable Polymers. *Ind. Eng. Chem. Res.* **2022**, *61* (13), 4648–4658.
(15) Muroga, J.; Kamio, E.; Matsuoka, A.; Nakagawa, K.; Yoshioka, T.; Matsuyama, H. Development of an Ion Gel-Based CO2 Separation Membrane Composed of Pebax 1657 and a CO2-Philic Ionic Liquid. *RSC Adv.* **2024**, *14* (29), 20786–20796.
(16) Cowan, M. G.; Gin, D. L.; Noble, R. D. Poly(Ionic Liquid)/Ionic Liquid Ion-Gels with High "Free" Ionic Liquid Content: Platform Membrane Materials for CO2/Light Gas Separations. *Acc. Chem. Res.* **2016**, *49* (4), 724–732.
(17) Zhang, J.; Kamio, E.; Matsuoka, A.; Nakagawa, K.; Yoshioka, T.; Matsuyama, H. Development of a Micro-Double-Network Ion Gel-Based CO2 Separation Membrane from Nonvolatile Network Precursors. *Ind. Eng. Chem. Res.* **2021**, *60* (34), 12640–12649.
(18) Liu, J.; Yang, X.; Xu, M.; Zhu, H.; Cheng, Y.; Li, S.; Li, T.; Jiao, Y.; Song, H. Highly Stretchable, Self-Adhesive, Ambient-Stable, and Wide-Temperature Adaptable Hydrophobic Ionogels for Wearable Strain Sensors. *J. Mater. Chem.* **2023**, *11* (3), 1184–1196.
(19) Xu, L.; Huang, Z.; Deng, Z.; Du, Z.; Sun, T. L.; Guo, Z.-H.; Yue, K. A Transparent, Highly Stretchable, Solvent-Resistant, Recyclable Multifunctional Ionogel with Underwater Self-Healing and Adhesion for Reliable Strain Sensors. *Adv. Mater.* **2021**, *33* (51), e2105306.
(20) Shi, P.; Wang, Y.; Tjiu, W. W.; Zhang, C.; Liu, T. Highly Stretchable, Fast Self-Healing, and Waterproof Fluorinated Copolymer Ionogels with Selectively Enriched Ionic Liquids for Human-Motion Detection. *ACS Appl. Mater. Interfaces* **2021**, *13* (41), 49358–49368.
(21) Son, Y. J.; Bae, J. W.; Lee, H. J.; Bae, S.; Baik, S.; Chun, K.-Y.; Han, C.-S. Humidity-Resistive, Elastic, Transparent Ion Gel and Its Use in a Wearable, Strain-Sensing Device. *J. Mater. Chem. A Mater. Energy Sustain.* **2020**, *8*, 6013–6021.
(22) Kamiyama, Y.; Tamate, R.; Hiroi, T.; Samitsu, S.; Fujii, K.; Ueki, T. Highly Stretchable and Self-Healable Polymer Gels from Physical Entanglements of Ultrahigh–Molecular Weight Polymers. *Sci Adv* **2022**, *8* (42), eadd0226.
(23) Kamiyama, Y.; Tamate, R.; Fujii, K.; Ueki, T. Controlling Mechanical Properties of Ultrahigh Molecular Weight Ion Gels by Chemical Structure of Ionic Liquids and Monomers. *Soft Matter* **2022**, *18*, 8582–8590.

(24) Shaplov, A. S.; Marcilla, R.; Mecerreyes, D. Recent Advances in Innovative Polymer Electrolytes Based on Poly(Ionic Liquid)s. *Electrochim. Acta* **2015**, *175*, 18–34.
(25) Mizutani, Y.; Watanabe, T.; Lopez, C. G.; Ono, T. Controlled Mechanical Properties of Poly(Ionic Liquid)-Based Hydrophobic Ion Gels by the Introduction of Alumina Nanoparticles with Different Shapes. *Soft Matter* **2024**, *20* (7), 1611–1619.
(26) Watanabe, T.; Oe, E.; Mizutani, Y.; Ono, T. Toughening of Poly(Ionic Liquid)-Based Ion Gels with Cellulose Nanofibers as a Sacrificial Network. *Soft Matter* **2023**, *19* (15), 2745–2754.
(27) Watanabe, T.; Takahashi, R.; Ono, T. Preparation of Tough, Thermally Stable, and Water-Resistant Double-Network Ion Gels Consisting of Silica Nanoparticles/Poly(Ionic Liquid)s through Photopolymerisation of an Ionic Monomer and Subsequent Solvent Removal. *Soft Matter* **2020**, *16* (6), 1572–1581.
(28) Zhang, H.; Li, M.; Yang, B. Design, Synthesis, and Analysis of Thermophysical Properties for Imidazolium-Based Geminal Dicationic Ionic Liquids. *J. Phys. Chem. C Nanomater. Interfaces* **2018**, *122* (5), 2467–2474.
(29) Nakajima, H.; Ohno, H. Preparation of Thermally Stable Polymer Electrolytes from Imidazolium-Type Ionic Liquid Derivatives. *Polymer (Guildf.)* **2005**, *46* (25), 11499–11504.
(30) Haddad, B.; Villemin, D.; Belarbi, E.-H.; Bar, N.; Rahmouni, M. New Dicationic Piperidinium Hexafluorophosphate ILs, Synthesis, Characterization and Dielectric Measurements. *Arab. J. Chem.* **2014**, *7* (5), 781–787.
(31) Choi, U. H.; Ye, Y.; Salas de la Cruz, D.; Liu, W.; Winey, K. I.; Elabd, Y. A.; Runt, J.; Colby, R. H. Dielectric and Viscoelastic Responses of Imidazolium-Based Ionomers with Different Counterions and Side Chain Lengths. *Macromolecules* **2014**, *47* (2), 777–790.
(32) Mogurampelly, S.; Ganesan, V. Ion Transport in Polymerized Ionic Liquid–Ionic Liquid Blends. *Macromolecules* **2018**, *51* (23), 9471–9483.

For Table of Contents Only